Cellular Signalling 26 (2014) 657–663

Contents lists available at ScienceDirect

Cellular Signalling

journal homepage: www.elsevier.com/locate/cellsig

Structural basis for the design of selective phosphodiesterase 4B inhibitors

David Fox 3rd [a], Alex B. Burgin [a], Mark E. Gurney [b,c,*]

[a] Emerald Bio, Bainbridge Island, WA, USA
[b] Tetra Discovery Partners, Grand Rapids, MI, USA
[c] Basic Pharmaceutical Sciences, West Virginia University, Morgantown, WV, USA

ARTICLE INFO

Article history:
Received 4 November 2013
Received in revised form 4 December 2013
Accepted 11 December 2013
Available online 19 December 2013

Keywords:
Phosphodiesterase-4B
PDE4B
Inhibitor
Control helix
Anti-inflammatory

ABSTRACT

Phosphodiesterase-4B (PDE4B) regulates the pro-inflammatory Toll Receptor –Tumor Necrosis Factor α (TNFα) pathway in monocytes, macrophages and microglial cells. As such, it is an important, although under-exploited molecular target for anti-inflammatory drugs. This is due in part to the difficulty of developing selective PDE4B inhibitors as the amino acid sequence of the PDE4 active site is identical in all PDE4 subtypes (PDE4A-D). We show that highly selective PDE4B inhibitors can be designed by exploiting sequence differences outside the active site. Specifically, PDE4B selectivity can be achieved by capture of a C-terminal regulatory helix, now termed CR3 (Control Region 3), across the active site in a conformation that closes access by cAMP. PDE4B selectivity is driven by a single amino acid polymorphism in CR3 (Leu674 in PDE4B1 versus Gln594 in PDE4D). The reciprocal mutations in PDE4B and PDE4D cause a 70–80 fold shift in selectivity. Our structural studies show that CR3 is flexible and can adopt multiple orientations and multiple registries in the closed conformation. The new co-crystal structure with bound ligand provides a guide map for the design of PDE4B selective anti-inflammatory drugs.

1. Introduction

Studies of targeted PDE4 gene deletions in mice by Jin and Conti, as well as others, have shown that the different PDE4 enzymes have non-redundant functions [1–6]. PDE4 is encoded by four different genes (PDE4A, PDE4B, PDE4C and PDE4D). These differ in their pattern of expression in the body, and differ in their pattern of targeting to subcellular compartments. The PDE4 family are the primary cAMP hydrolyzing enzymes in cells, and as such, shape the spatial and temporal patterning of cAMP signaling within cellular microdomains.

PDE4B is a well-validated target for modulating inflammation. For example, tumor necrosis factor (TNF-α) production by macrophages in response to an inflammatory stimulus is mediated by the Toll receptor pathway through an increase in PDE4B gene expression [2,3]. The increase in PDE4B drives down cAMP levels in the macrophage, thereby causing an increase in TNFα production. PDE4B is the major PDE4 in macrophages, and deletion of PDE4B in mice blunts the production of TNFα in response to inflammatory stimuli. PDE4B selective inhibitors similarly suppress TNF-α production in rodent models [7]. PDE4B dysregulation may also be important in psychiatric disease [8].

Each PDE4 gene encodes multiple transcripts that produce three isoforms of the enzyme termed long, short and super short. Long isoforms of PDE4 contain two upstream control regions known as UCR1 and UCR2 (upstream conserved region 1 and 2). These form a negative regulatory module which is relieved by protein kinase A (PKA) phosphorylation of UCR1 in response to cAMP (Fig. 1A) [9]. Burgin et al. demonstrated that this negative regulation resulted from a control helix within the UCR2 domain that can close over the active site [10]. The "closed" UCR2 conformation was visualized by X-ray crystallography using small molecules that bound in the active site and simultaneously interacted with specific residues in UCR2, most importantly Phe196. This residue is not conserved among PDE4 genes. Instead, it is replaced by a tyrosine in PDE4A-C. This has allowed the discovery of a number of PDE4D selective inhibitors which exploit the UCR2 binding pose (*e.g.* RS25344, PMNPQ, and D159153).

In the absence of UCR2, we showed previously that PMNPQ captures a second, downstream C-terminal helix, now termed CR3 (Conserved Region 3). CR3 is present in the protein constructs used to crystallize the catalytic domain of PDE4 but is typically disordered within the crystal lattice presumably because the helix only weakly interacts with the catalytic domain by itself. CR3 is visible in a number of PDE4 catalytic domain structures (1F0J, 3HMV, 3W5E and 3KKT); however, the length of CR3 that is visible is variable as is the orientation of CR3 in the structure [11–13].

To better understand the role of CR3 in regulating PDE4 activity, we surveyed additional compounds that could bind and stabilize CR3 over the active site. We report here the analysis and X-ray crystal structure

Abbreviation: CR3, Control Region 3.

* Corresponding author at: Tetra Discovery Partners, Grand Rapids, MI, USA.
E-mail address: mark@tetradiscovery.com (M.E. Gurney).

0898-6568
http://dx.doi.org/10.1016/j.cellsig.2013.12.003

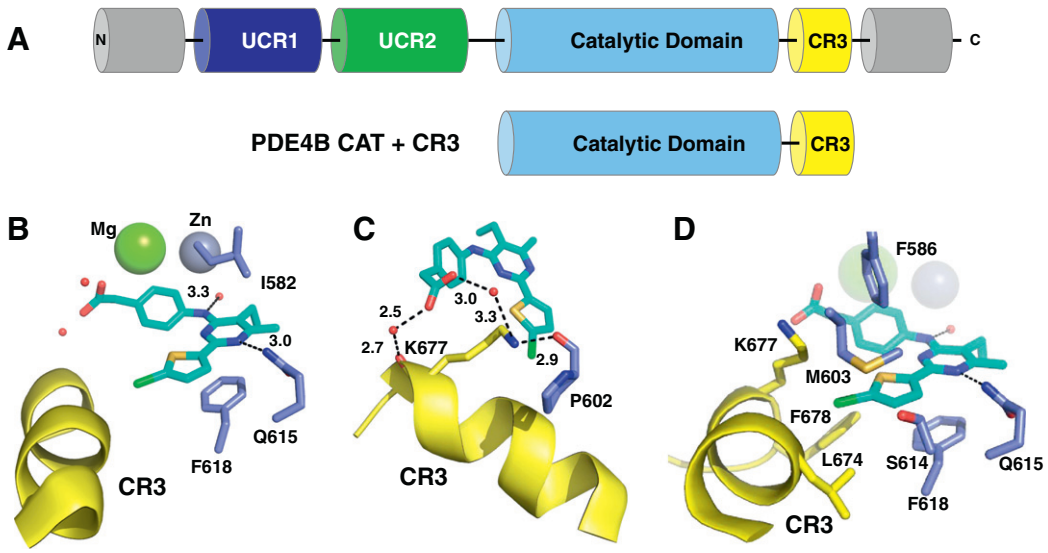

Fig. 1. PDE4B selective inhibitor captures the C-terminal CR3 by novel binding mode. A. Domain architecture for full-length PDE4 and the crystallization construct (PDE4B CAT + CR3). **B–D.** A-33 (cyan) interaction with catalytic domain (blue) and CR3 (yellow). **B.** "P-clamp" and "Q-switch." **C.** Hydrogen bonding network bridging CR3 and A-33 carboxylic acid. **D.** Hydrophobic interactions with A-33 thiophene. Atom coloring — Oxygen (red), Nitrogen (blue), Carbon (cyan), Chloride (green), and Sulfur (yellow). Metals are shown as large spheres (Mg^{2+} - green and Zn^{2+} - silver) and waters are shown as small red spheres. Hydrogen-bonds are represented by black dashed lines. PDB: 4MYQ.

of a previously described 2-arylpyrimidine [7] derivative (compound 33, herein referred to a A-33) bound to PDE4B. Comparison of this structure with the PMNPQ-PDE4D (PDB: 3G58), NVW-PDE4B (PDB: 3W5E), and OCP-PDE4B (PDB: 3KKT) structures, shows that small molecules can interact with different residues along the CR3 helix resulting in multiple "closed" conformations. The CR3 helix can adopt slightly different orientations across the active site, each with unique helical registries; however, only in the conformation observed in the new A-33 structure do the sequence differences between the PDE4B and PDE4D enzymes become critical for this interaction. In support of this model, we show that the reciprocal exchange of a single amino acid residue in CR3 between the PDE4B and 4D long isoforms can convert the selectivity profile of A-33 for PDE4B into that of PDE4D, and vice versa. These results demonstrate that CR3 can regulate PDE4 activity in biologically relevant PDE4 isoforms, and enable the first structure based drug design program of PDE4B selective inhibitors.

2. Materials and methods

2.1. PDE4 protein constructs

PDE4D residue numbering is based on the reference PDE4D3 isoform, GenBank accession No. AAA97892, and PDE4B residue numbering is on the reference PDE4B3, GenBank accession No. Q07343. Methods used to generate synthetic genes for human PDE4B1 (Swiss-Prot: Q07343.1) and PDE4D7 (GenBank: AAN10118.1) constructs are as described in Burgin et al. [10]. Mutations in the PDE4B1 (L674Q) and PDE4D7 (Q594L) constructs were cloned by site-directed mutagenesis of the respective long-form construct. A synthetic gene encoding the PDE4B catalytic domain and CR3 element (PDE4B-CR3, residues 324–691) with amino-terminal thrombin cleavable hexahistidine tag was engineered for Baculovirus-infected insect cell expression using Gene Composer™ software (Emerald Bio, Bainbridge Island, WA) [14]. The 389 amino acid fragment was cloned into a BV transfer vector, expression from which is driven by the polh promoter, using 5′ BamHI and 3′ HindIII.

2.2. Expression and purification of PDE4 proteins

PDE4 constructs were transfected into Sf9 insect cells (Expression Systems) using BestBac 2.0, v-cath/chiA Deleted Linearized Baculovirus DNA (Expression Systems). Virus from each transfection was amplified through 4 rounds to produce virus stock for large scale production. The large scale preparations were grown in ESF921 medium (Expression Systems) of approximately $2.5e^6$ cells per ml that was infected with 10% final virus (75 ml) and harvested 48 h post-infection. Cells were centrifuged to collect cell paste which was frozen drop-wise into liquid nitrogen and stored at −80 °C.

Frozen cell paste of the PDE4 long form and catalytic domain proteins was resuspended and lysed hypotonically in 20 mM tris(hydroxymethyl) aminomethane (Tris) pH 8.0 containing one complete protease inhibitor tablet for one hour at 4 °C. The lysate was clarified by centrifugation at 42 K rpm for 45 min at 4 °C. Sodium chloride (NaCl) was added to the clarified lysate to obtain a final concentration of 0.5 M. Clarified lysate was first purified by immobilized metal affinity chromatography with a HiTrap™ Chelating HP column and an AKTA FPLC system. The protein was eluted over a gradient with 20 mM Tris pH 8.0, 0.5 M NaCl and 0.5 M imidazole and the eluted fractions were analyzed via SDS-PAGE prior to pooling. Long-form PDE4 proteins were dialyzed into the final buffer containing 20 mM TRIS at pH 8.0, 0.1 M NaCl, 0.1 mM $MgCl_2$, 0.1 mM $ZnCl_2$, and 2 mM dithiothreitol (DTT) and then flash frozen with liquid nitrogen in aliquots of 0.5 mL at 0.1 mg/ml as measured by A_{280}. The PDE4B-CR3 protein eluted pool was further treated with thrombin to cleave the 6X His tag followed by removal of thrombin and the cleaved fusion tag by passing the cleaved pool over a benzamidine column and a HiTrap™ Chelating HP column in series. Cleaved PDE4B-CR3 was collected in the flow-through and dialyzed into the final buffer containing 20 mM 4-(2-hydroxyethyl)-1-piperazineethanesulfonic acid (HEPES) pH 7.5, 100 mM NaCl and 1 mM DTT. Cleaved PDE4B-CR3 was concentrated via centrifugal concentration to a final concentration of 7.9 mg/ml as measured by A_{280}. All proteins were stored at −80 °C.

2.3. Co-crystallization of PDE4B with A-33

Crystals of PDE4B-CR3 were grown by sitting drop vapor diffusion at 295 K using 0.5 μl of 7.9 mg/ml protein in the presence of 0.5 mM A-33 (DMSO) and combined with 0.5 μl of crystallization buffer containing 328.6 mM potassium formate, 24% w/v PEG 3,350 (based on $JCSG^+$ condition A10) [15]. Crystals grown for data collection were streak seeded using crystals described above and were cryo-protected using 20% ethylene glycol mixed with 0.1 mM A-33.

2.4. Structure determination by X-ray crystallography

A 1.90 Å dataset of a co-crystal of human PDE4B-CR3 and compound A-33 was collected in-house at Emerald BioStructures on a Rigaku SuperBright FR-E + X-ray generator with Osmic VariMax HF optics and a Saturn 944+ CCD detector. Diffraction data were reduced and scaled with XDS/XSCALE [16]. The structure of PDE4B-CR3 bound to A-33 was solved by molecular replacement using pre-existing structures of the PDE4B catalytic domain (PDB: 3G45) [10]. The structure was refined using iterative cycles of TLS and restrained refinement with REFMAC5 [17], part of the CCP4 program suite [18], and model-building using the Crystallographic Object-Oriented Toolkit (COOT) [19]. The structure was peer-reviewed internally and validated using Molprobity [20] prior to deposition in the Protein Data Bank (PDB: 4MYQ) [21,22]. Diffraction data and refinement statistics are listed in Table 1.

2.5. Kinetic assay of PDE4 activity.

Kinetic assay of cAMP hydrolysis by purified PDE4 is measured by coupling the formation of the PDE4 reaction product, 5′-adenosine monophosphate to the oxidation of reduced nicotinamide adenine dinucleotide (NADH) by the use of three coupling enzymes (yeast myokinase, pyruvate kinase and lactate dehydrogenase), which allows fluorescent determination of reaction rates [10]. Assays are performed in 96-well plates in a total volume of 200 μl/well. Compounds are dissolved in dimethylsulfoxide (DMSO) and added to plates in a volume of 10 μl followed by addition of 165 μl of assay mix. Plates are pre-incubated at 25 °C for 15 min and the reactions are initiated by the addition of 25 μl of cAMP followed by thorough mixing. Reaction rates are measured by monitoring the decrease in fluorescence using excitation at 355 nm and emission at 460 nm for a period of 10 min in a fluorescence plate reader. Initial rates (slopes) are determined from linear portions of the progress curves. Final concentrations of assay components are as follows: 50 mM Tris, pH 8, 10 mM $MgCl_2$, 50 mM KCl, 2% DMSO, 5 mM tris(2-carboxyethyl)phosphine (TCEP), 0.4 mM phosphenolpyruvate (PEP), 0.01 mM NADH, 0.04 mM adenosine triphosphate (ATP), 0.004 mM cAMP, 7.5 units myokinase from yeast, 1.6 units pyruvate kinase, 2 units lactate dehydrogenase, and ~10 nM PDE4. The concentration of purified PDE4 in the assay was adjusted to yield an initial rate of approximately −0.7 RFU/s. All data are percent normalized relative to controls and are presented as percent inhibition. An inhibitory concentration 50% (IC_{50}) value is calculated by fitting a sigmoidal dose response curve. Z′ quality factors are >0.6 for the assay. Human PDE4D7 contained a mutation of S54D to mimic activation by cAMP-dependent protein kinase A (PKA) and S579A/S581A to remove the potential for ERK-dependent phosphorylation. Human PDE4B1 also contained the corresponding mutations S133D (PKA) and S659A/S661A (ERK).

Table 1
Diffraction data and refinement statistics.

PDB ID	4MYQ
Parameter	Overall (Highest shell)
Protein	VCID 6271 (PDE4B-CR3)
Ligand	A-33
Beamline	Rotating anode
Data collection	
Collection date	16-Mar-2012
Space group	$P4_2$
Unit cell	a = b = 99.7 Å, c = 47.0 Å α = β = γ = 90°
# molecules/asymmetric unit	1
Wavelength	1.5418
Solvent content	55.6%
V_m	2.7 $Å^3$/Da
Resolution	50.0-1.90 Å (1.95-1.90)
I/σI	12.50 (2.29)
Completeness	97.3% (86.7%)
R_{merge}	0.087 (0.483)
Multiplicity	3.30 (1.50)
Unique	35,759 (2,326)
Mosaicity	0.30
Refinement statistics	
Reflections	35,749 (2,117)
No. of non-hydrogen atoms	3,223
Resolution	49.85-1.90 Å (1.95-1.90)
R_{cryst}	0.190 (0.365)
R_{free}	0.222 (0.401)
FreeR # of reflections	5%, 1,788 (117)
Average B-factor ($Å^2$)	12.80
Model geometry	
Bond length deviation (Å)	0.014
Bond angle deviation (°)	1.487
Ramachandran	
Favored	98.53%
Allowed	100.0%
Molprobity score	99th percentile

3. Results

Naganuma et al. discovered a series of arylpyrimidine PDE4 inhibitors (*e.g.* A-33) with >100X selectivity for PDE4B versus PDE4D [7]. We showed separately that the observed affinity and selectivity were dependent on the presence of sequences C-terminal to the catalytic domain, which we now term "control region 3" (CR3) [23]. To understand the structural basis of this selectivity, we attempted co-crystallization trials with PDE4B catalytic domain constructs containing CR3, but lacking UCR2, and obtained crystals that diffracted X-rays to 1.9 Å resolution (Fig. 1A). The resulting structure shows that A-33 makes multiple interactions with the catalytic domain and simultaneously with residues from CR3 (Fig. 1B). A-33 binds the PDE4B catalytic domain with its central pyrimidine ring stacked between Phe618 and Ile582 and in position to hydrogen bond to Gln615. These constitute the "P clamp" and "Q switch" interactions observed among all PDE4 inhibitors as described by Card et al. [24]. The amine linker between the central core and the arylcarboxymethyl group also makes a hydrogen bond to a conserved water molecule constituting part of the hydration shell of the catalytic metals. Finally, the ethyl and methyl substituents off of the central pyrimidine ring provide shape complementarity to the Q1 hydrophobic pocket in the back of the active site. This model explains why substituents at all of these positions are critical for potency but have little effect on PDE4B vs. PDE4D selectivity [24], since the same pockets are conserved in both active sites.

Naganuma et al. previously showed that the primary substituents responsible for PDE4B selectivity are the thienyl and arylcarboxymethyl substituents [7]. Our X-ray crystal structure shows that these groups specifically interact with residues from CR3. The chloro-substituted thienyl group of A-33 fills the Q2 pocket (Fig. 1D) at the interface between the catalytic domain (Met603, Phe618, and the backbone Ser614) and CR3 (Lys677, Phe678 and Leu674). The carboxylic acid moiety makes a water-mediated hydrogen bond contact to the main-chain carbonyl of Lys677 (Fig. 1C), and the acid group makes a second water-mediated hydrogen bond to the amine of Lys677, although the distances are slightly longer than expected for an ideal interaction. The amine of Lys677 directly ties CR3 to the catalytic domain through a second hydrogen bond to the main-chain carbonyl of Pro602 on the catalytic domain. Even weak interactions that would help position and stabilize this Lys677-Pro602 interaction would be expected to have a significant effect on the overall binding energy of the closed complex (A-33/catalytic domain/CR3). Together, these results show that A-33 has good shape complementarity as an interface between the catalytic domain and CR3 and makes multiple hydrophobic and polar interactions with both domains. This holds CR3 in a "closed conformation" that blocks substrate binding.

Multiple groups previously described small molecule inhibitors that bind in the active site and engage CR3 (Fig. 2). For example, Burgin et al. demonstrated that PMNPQ can bind the catalytic domain of PDE4D and interact with CR3. The PMNPQ–CR3 interaction is only observed when UCR2 is absent, which does not occur in any biological isoform of PDE4. Otherwise, PMNPQ preferentially captures UCR2 and holds it across the active site. In a second example, Goto et al. co-crystallized a pyrimidine sulfone (NVW) bound to the PDE4B catalytic domain which engages CR3 (PDB: 3W5E). This compound has a very similar binding mode as the pyrimidinone, CP-80633 (OCP) [25], which also co-crystallizes with CR3 of PDE4B (PDB: 3KKT, unpublished).

Comparison of the A-33 structure (PDB: 4MYQ) with the published PMNPQ (PDB: 3G58), NVW (PDB: 3W5E), and OCP (PDB: 3KKT) crystal structures shows that the CR3 helices have different orientations over the active site (Fig. 2). The Cα carbons of CR3 from NVW (orange) and OCP (green) are nearly superimposable but distinctly different in orientation from the CR3 backbones in the A-33 (yellow) or PMNPQ (magenta) structures. In addition, although the A-33 and PMNPQ CR3 helices are nearly superimposable, these helices are rotated relative to one another by a single helical turn. Altogether, this results in three different helical poses (Fig. 3B, C and D). As a result, the three different helical poses present different amino acid residues and, therefore, different shapes and functional groups to the active site. The different poses are presumably selected by chemical differences between the inhibitors, and we hypothesize that the A-33 registry places amino acid differences between PDE4B vs. PDE4D into a context that can affect selectivity.

The PDE4D-CR3 helical register as captured by PMNPQ places Phe598 toward the ligand interface at the same relative position as Leu674 in the A-33 structure. It also points Lys597 (homologous to PDE4B Lys677) away from the binding interface and prevents the critical water-mediated hydrogen bond interaction observed with A-33. If the CR3 α-helix of PDE4D is placed in the PDE4B A-33 register, with PDE4D Lys597 occupying the same relative position as PDE4B Lys677, then PDE4D Gln594 faces the binding interface and Phe598 sterically clashes with the chloro group from the thienyl moiety of A-33 (Fig. 4A). Likewise, the PDE4D catalytic domain with PMNPQ bound, when modeled with CR3 from PDE4B, suggests that the nitro group from the phenyl moiety of PMNPQ would sterically clash with Leu674 of CR3 from PDE4B (not shown).

Comparison of the A-33 structure with the NVW and OCP-bound structures shows that a two-residue shift in the helical registry brings Leu674, Met675, and Phe678 to the interface with the ligand (NVW and OCP) in the active site instead of Leu674, Lys677 and Phe678 (A-33). An overlay of the PDE4B catalytic domains shows that the chloro substitution on the A-33 thienyl ring sterically clashes with Phe678 if CR3 adopts the alternative pose (Fig. 4B and C). In addition, NVW and OCP do not have moieties that can interact and stabilize the CR3 pose observed in the A-33 structure. Together, these results show that each CR3 pose is stabilized by unique interactions with ligands bound in the active site, and specific interactions are predicted to destabilize alternative poses. These results emphasize that the CR3 helix is very flexible. It is possible that additional small molecules could stabilize alternative CR3 poses.

If the X-ray crystal structure reflects binding in a biological isoform, it should explain why A-33 is >100× selective for PDE4B vs. PDE4D. There are several non-conserved residues between PDE4D and PDE4B within CR3 that could contribute to selectivity (highlighted in red in Fig. 3A); however, there are only two residues (PDE4B Leu674/PDE4D Gln594 and PDE4B Met675/PDE4D Thr595) that are in position to engage the ligand and/or catalytic domain. In the model, Leu674 interacts with the wall of the catalytic domain and with the thienyl group on A-33. This provides a uniquely closed hydrophobic environment for the compound, which we hypothesize, contributes to PDE4B selectivity. Met675 is adjacent to the face of the catalytic domain; however, a threonine at this position would not be expected to be detrimental to the overall CR3 pose. If the glutamine vs. leucine difference is the basis for selectivity, mutation of Gln594 → Leu (Q594L) in PDE4D should increase A-33 potency, and conversely, the mutation Leu674 → Gln (L674Q) in PDE4B should decrease A-33 potency. To test this hypothesis, we placed these mutations in the physiological context of the long splice isoforms, PDE4D7 and PDE4B1, which contain both N-terminal regulatory domains (UCR1, with PKA phosphomimetic mutation S → D [10], & UCR2) and CR3. Indeed, the single amino acid change shifts A-33 IC_{50} from 1569 nM against PDE4D7 (wild-type CR3) to 21 nM against PDE4D7 Q594L (Fig. 5A). The reciprocal mutation in PDE4B1 shifts A-33 IC_{50} from 32 nM against PDE4B1 (wild-type CR3) to 2035 nM against PDE4B1 L674Q. These results indicate that the large degree of PDE4B selectivity is due to this single amino acid difference between PDE4B and PDE4D.

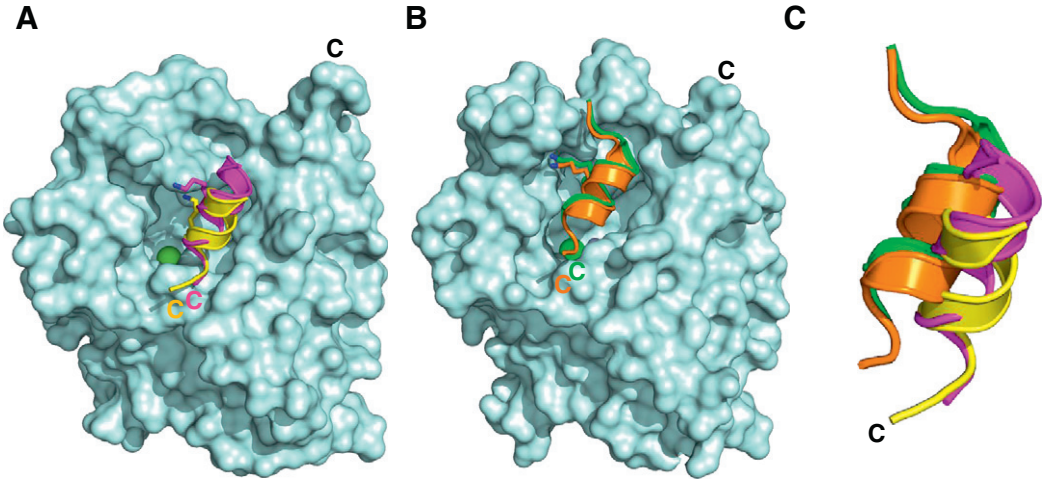

Fig. 2. PDE4 inhibitors capture unique CR3 poses over the catalytic domain. A. PDE4B catalytic domain is shown as a surface representation (cyan, PDB: 4MYQ) with the A-33 captured CR3 helix (yellow-ribbon) and overlaid with the PMNPQ captured CR3 helix (magenta-ribbon) from PDE4D. **B.** PDE4B catalytic domain (PDB: 3W5E) with the NVW captured CR3 helix (orange-ribbon) and overlaid with the OCP captured CR3 helix (green-ribbon). **C.** Comparison of CR3 poses from the A-33, PMNPQ, NVW and OCP, colored as in A–B. C-termini of catalytic domain and CR3 helices are indicated. Small molecules are removed from the figure for simplicity, but the catalytic metals are highlighted in the active site (Mg^{2+} - green, Zn^{2+} - silver). Lys677 (PDE4B)/Lys597 (PDE4D) are shown as sticks to illustrate relative CR3 helical registry captured by each inhibitor.

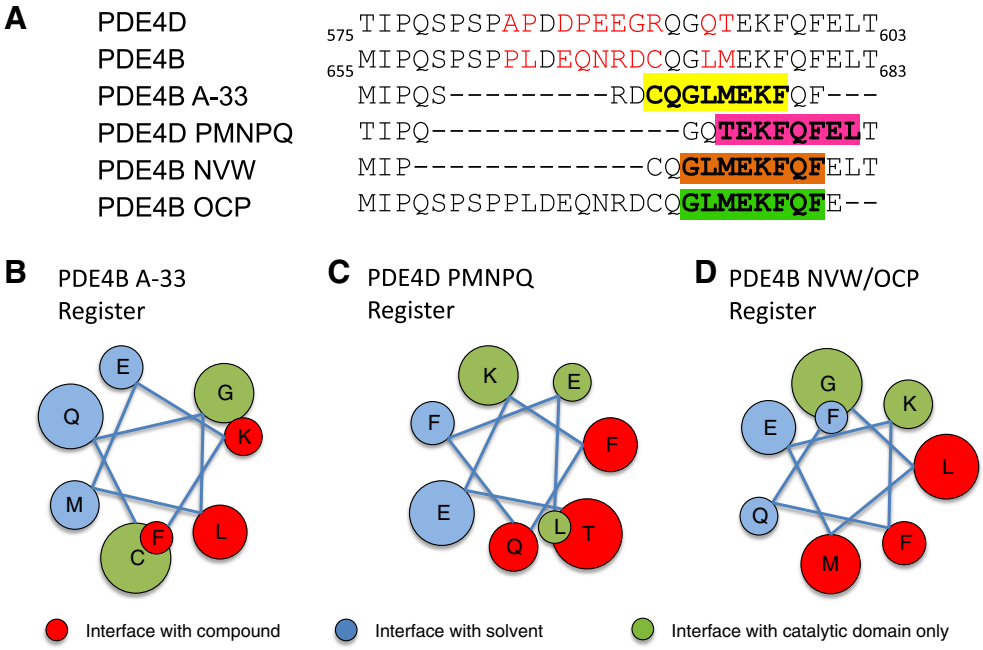

Fig. 3. PDE4B inhibitor A-33 selects a specific CR3 pose. A. Sequence alignment of CR3. Top two lines show the long-form sequences for PDE4D (669–683) and PDE4B (589–603); non-conserved amino acids are highlighted in red. Amino acid residues that can be modeled in the A-33, PMNPQ, NVW and OCP structures are shown (colored as in Fig. 2). **B–D.** Helical wheel representations are shown for the CR3 helices captured by **(B)** A-33, **(C)** PMNPQ, and **(D)** NVW/OCP. Helical wheel residue coloring: compound interface (red), catalytic domain interface (green), and solvent interface (blue).

4. Discussion

We have obtained a 1.9 Å resolution crystal structure of A-33 [7] bound in the active site of PDE4B while simultaneously stabilizing a C-terminal α-helix across the active site (now termed Control Region 3, "CR3"), thereby locking the enzyme in an inactive "closed" conformation. This result mirrors N-terminal UCR2 structures that have been exploited to develop PDE4D-selective allosteric modulators [10]. These preferentially interact with a non-conserved phenylalanine residue (tyrosine in PDE4B). The PDE4B-selective inhibitor A-33 displays the typical P-clamp and Q-switch interactions previously described for all PDE4 active site inhibitors [24]; however, A-33 also contains a carboxylic acid moiety which reaches out of the active site and engages CR3 through water mediated contacts. In addition, a chloro-substituted thienyl group provides excellent shape complementarity with a pocket formed between CR3 and the catalytic domain further stabilizing the CR3 helix over the active site. Comparison of the A-33 structure with other PDE4 structures, in which CR3 is visible, that is, when CR3 is stabilized by a small molecule ligand, clearly shows that CR3 is flexible and can adopt multiple orientations and multiple registries. Each small molecule presents different chemical features that stabilize different poses of CR3. Most importantly, A-33 stabilizes a unique pose of CR3 over the active site that results in a non-conserved residue (Leu674) interacting with both A-33 and the face of the catalytic domain. Mutagenesis studies show that this CR3 pose is destabilized in the PDE4D background resulting in PDE4B-selectivity.

Together, these results show that it is possible to generate highly selective PDE4B inhibitors by exploiting sequence differences outside of the catalytic domain. Although not yet described, it is possible that small molecules could be developed that preferentially interact with the non-conserved tyrosine in UCR2 to generate PDE4B-selective inhibitors. Similarly, because of the high degree of flexibility of CR3, it is possible that small molecules could be developed that preferentially stabilize a CR3 conformation that would be unique to PDE4D. Despite the fact that the active sites of all PDE4 enzymes are completely conserved, there exist multiple structure-based design approaches to create highly specific inhibitors by exploiting non-conserved residues within the UCR2 and CR3 regulatory domains.

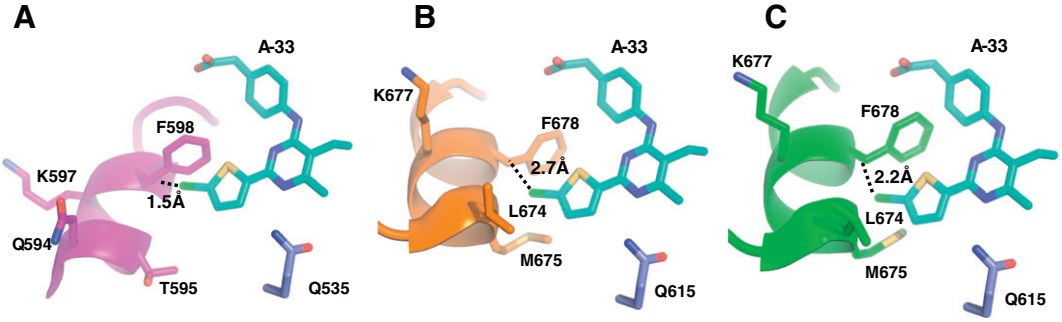

Fig. 4. Modeling of other CR3 registries shows de-selection by A-33. A. A-33 overlaid with the PDE4D-CR3 helix predicts a clash with Phe598. **B–C.** A-33 overlaid with the PDE4B-CR3 helix registry captured by **(B)** NVW and **(C)** OCP predicts a clash with Phe678. CR3 helices and selected residues are colored as shown in Fig. 2. A-33 (cyan) and invariant Gln615 (PDE4B)/Gln535 (PDE4D) (blue) are shown as sticks.

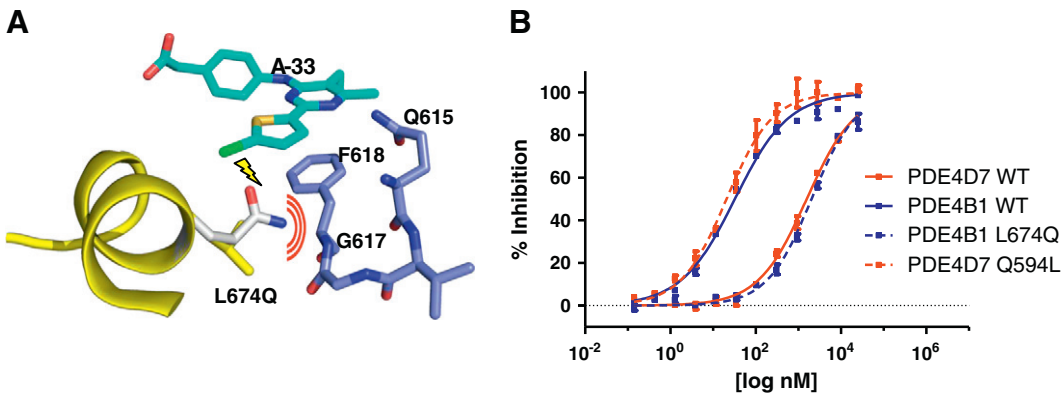

Fig. 5. A-33 selectivity for PDE4B is dependent on a single amino acid difference. A. Leu674Qln mutation was modeled (white) and predicts disruption of CR3 binding through 1) steric clash (red lines) with G617 of the catalytic domain, and 2) placement of a hydrophilic residue in a hydrophobic environment (lightning bolt). Coloring is as shown in Fig. 1. **B.** A-33 biochemical inhibition curves by PDE kinetic assay against PDE4D7, with wild-type CR3 (red, solid), PDE4D7 Q594L (red, dashed), PDE4B1, with wild-type CR3 (blue, solid), and PDE4B1 L674Q (blue, dashed).

The physiological importance of the regulation of PDE4D activity by UCR2 is underscored by human genetic data. Human PDE4D mutations have been described in children with acrodysostosis, a developmental disorder that causes mental retardation, short fingers and toes, and facial dysmorphia [26–28]. Acrodysostosis mutations map to UCR1, UCR2 and catalytic domain residues that interact with UCR2. Thus, the acrodysostosis mutations are proposed to activate PDE4D by destabilizing closure of UCR2 across the active site. Similar genetic support for the physiological role of CR3 in the regulation of PDE4D or PDE4B activity is not available. The CR3 helix may be important for RACK-1 binding (receptors for activated C-kinase); however, there is no change in K_m or V_{max} by RACK1-bound PDE4D5, so CR3 must be held in an open conformation [29,30]. It is also important to note that several other partner proteins including AKAP18 [31], ERK2 [32] and beta-arrestin [29,30] have been shown to bind a conserved "FQF" (Phe678-Gln679-Phe680) motif present on CR3. Analysis of the A-33 structure shows that these residues are not accessible in the closed conformation suggesting that these partner proteins would stabilize a CR3 open conformation. Additional experiments are needed to know if ligand binding would minimize partner protein interactions, or if the presence of partner proteins would mitigate ligand binding; however, it is interesting to speculate that in addition to being gene selective, ligands with binding modes similar to A-33 would provide another level of specificity by only engaging a specific subset of PDE4B-partner protein complexes *in vivo*.

The ability to use structures to guide the design of PDE4B-selective compounds acting through CR3 has very important implications for developing PDE4 therapeutics. Vomiting and emesis were suggested by Robichaud et al. to be associated with inhibition of PDE4D [33]. The association of PDE4D inhibition with emesis was corroborated by subsequent studies showing that selective PDE4D inhibitors are potent emetogens in multiple species [10,34]. Thus, it has been hypothesized that selective compounds targeting PDE4 isoforms other than PDE4D will have reduced emetic potential. Naganuma et al. report that A-33 has a very favorable ratio of anti-inflammatory activity in mice and high tolerability with respect to emesis in ferrets [7]. The structural results reported herein will facilitate the chemical optimization of small molecule PDE4B inhibitors for treating inflammatory and psychiatric diseases with reduced PDE4 family cross-reactivity.

5. Conclusions

Our structural and biochemical studies support inhibition of PDE4B activity by novel interactions between catalytic domain bound arylpyrimidine inhibitors and a C-terminal regulatory element known as CR3.

Sequence differences between the PDE4B and PDE4D CR3 domains allow for selective inhibition of PDE4B by small molecules that favor this new CR3 binding pose.

These data highlight the importance of engaging CR3 in a specific helical register to achieve PDE4B selectivity and will enable the structure-based design of PDE4B selective drugs for the treatment of inflammatory and psychiatric diseases.

Competing interests

The authors declare that they have no competing interests towards any aspect of the work described in this paper.

Acknowledgments

This study was funded by the National Institute of Mental Health award 1R43MH091791 to M.E.G. The authors would like to thank D. M. Dranow, P. Witte, J. Abendroth, K. Atkins, A. Raymond for contributions to the research and review of the manuscript and X. Mo and T. Hagen for the synthesis of A-33.

Author contributions

D.F. directed cloning, expression, purification, crystallization, data collection, solution of the PDE4B x-ray structures, and coauthored the manuscript; A.B.B directed construct design, crystallization and coauthored the manuscript; M.E.G. conducted the PDE4 enzyme assays, and coauthored the manuscript.

References

[1] G. Hansen, S. Jin, D.T. Umetsu, M. Conti, Proc. Natl. Acad. Sci. U. S. A. 97 (2000) 6751.
[2] S.L. Jin, M. Conti, Proc. Natl. Acad. Sci. U. S. A. 99 (2002) 7628.
[3] S.L. Jin, L. Lan, M. Zoudilova, M. Conti, J. Immunol. 175 (2005) 1523.
[4] Y.F. Li, Y.F. Cheng, Y. Huang, M. Conti, S.P. Wilson, J.M. O'Donnell, H.T. Zhang, J. Neurosci. 31 (2011) 172.
[5] H.T. Zhang, Y. Huang, A. Masood, L.R. Stolinski, Y. Li, L. Zhang, D. Dlaboga, S.L. Jin, M. Conti, J.M. O'Donnell, Neuropsychopharmacology 33 (2008) 1611.
[6] H.T. Zhang, Y. Huang, S.L. Jin, S.A. Frith, N. Suvarna, M. Conti, J.M. O'Donnell, Neuropsychopharmacology 27 (2002) 587.
[7] K. Naganuma, A. Omura, N. Maekawara, M. Saitoh, N. Ohkawa, T. Kubota, H. Nagumo, T. Kodama, M. Takemura, Y. Ohtsuka, J. Nakamura, R. Tsujita, K. Kawasaki, H. Yokoi, M. Kawanishi, Bioorg. Med. Chem. Lett. 19 (2009) 3174.
[8] J.K. Millar, B.S. Pickard, S. Mackie, R. James, S. Christie, S.R. Buchanan, M.P. Malloy, J.E. Chubb, E. Huston, G.S. Baillie, P.A. Thomson, E.V. Hill, N.J. Brandon, J.C. Rain, L.M. Camargo, P.J. Whiting, M.D. Houslay, D.H. Blackwood, W.J. Muir, D.J. Porteous, Science 310 (2005) 1187.
[9] J. Lim, G. Pahlke, M. Conti, J. Biol. Chem. 274 (1999) 19677.
[10] A.B. Burgin, O.T. Magnusson, J. Singh, J.M. Bjornsson, M. Thorsteinsdottir, S. Hrafnsdottir, T. Hagen, P. Witte, B.L. Staker, A.S. Kiselyov, L.J. Stewart, M.E. Gurney, Nat. Biotechnol. 28 (2010) 63.

[11] M. Kranz, M. Wall, B. Evans, A. Miah, S. Ballantine, C. Delves, B. Dombroski, J. Gross, J. Schneck, J.P. Villa, M. Neu, D.O. Somers, Bioorg. Med. Chem. 17 (2009) 5336.
[12] T. Goto, A. Shiina, T. Yoshino, K. Mizukami, K. Hirahara, O. Suzuki, Y. Sogawa, T. Takahashi, T. Mikkaichi, N. Nakao, M. Takahashi, M. Hasegawa, S. Sasaki, Bioorg. Med. Chem. Lett. 23 (2013) 3325.
[13] R.X. Xu, A.M. Hassell, D. Vanderwall, M.H. Lambert, W.D. Holmes, M.A. Luther, W.J. Rocque, M.V. Milburn, Y. Zhao, H. Ke, R.T. Nolte, Science 288 (2000) 1822.
[14] D. Lorimer, A. Raymond, J. Walchli, M. Mixon, A. Barrow, E. Wallace, R. Grice, A. Burgin, L. Stewart, BMC Biotechnol. 9 (2009) 36.
[15] J. Newman, D. Egan, T.S. Walter, R. Meged, I. Berry, M. Ben Jelloul, J.L. Sussman, D.I. Stuart, A. Perrakis, Acta Crystallogr. D Biol. Crystallogr. 61 (2005) 1426.
[16] W. Kabsch, Acta Crystallogr, D Biol. Crystallogr. 66 (2010) 125.
[17] G.N. Murshudov, P. Skubak, A.A. Lebedev, N.S. Pannu, R.A. Steiner, R.A. Nicholls, M.D. Winn, F. Long, A.A. Vagin, Acta Crystallogr, D Biol. Crystallogr. 67 (2011) 355.
[18] M.D. Winn, C.C. Ballard, K.D. Cowtan, E.J. Dodson, P. Emsley, P.R. Evans, R.M. Keegan, E.B. Krissinel, A.G. Leslie, A. McCoy, S.J. McNicholas, G.N. Murshudov, N.S. Pannu, E.A. Potterton, H.R. Powell, R.J. Read, A. Vagin, K.S. Wilson, Acta Crystallogr, D Biol. Crystallogr. 67 (2011) 235.
[19] P. Emsley, B. Lohkamp, W.G. Scott, K. Cowtan, Acta Crystallogr, D Biol. Crystallogr. 66 (2010) 486.
[20] V.B. Chen, W.B. Arendall III, J.J. Headd, D.A. Keedy, R.M. Immormino, G.J. Kapral, L.W. Murray, J.S. Richardson, D.C. Richardson, Acta Crystallogr, D Biol. Crystallogr. 66 (2010) 12.
[21] H. Berman, K. Henrick, H. Nakamura, Nat. Struct. Biol. 10 (2003) 980.
[22] H.M. Berman, J. Westbrook, Z. Feng, G. Gilliland, T.N. Bhat, H. Weissig, I.N. Shindyalov, P.E. Bourne, Nucleic Acids Res. 28 (2000) 235.
[23] M.E. Gurney, A.B. Burgin, O.T. Magnusson, L.J. Stewar, Handbook of experimental pharmacology, 2011. 167.
[24] G.L. Card, B.P. England, Y. Suzuki, D. Fong, B. Powell, B. Lee, C. Luu, M. Tabrizizad, S. Gillette, P.N. Ibrahim, D.R. Artis, G. Bollag, M.V. Milburn, S.H. Kim, J. Schlessinger, K.Y. Zhang, Structure 12 (2004) 2233.
[25] V.L. Cohan, H.J. Showell, D.A. Fisher, C.J. Pazoles, J.W. Watson, C.R. Turner, J.B. Cheng, J. Pharmacol. Exp. Ther. 278 (1996) 1356.
[26] D.C. Lynch, D.A. Dyment, L. Huang, S.M. Nikkel, D. Lacombe, P.M. Campeau, B. Lee, C.A. Bacino, J.L. Michaud, F.P. Bernier, F.C. Consortium, J.S. Parboosingh, A.M. Innes, Hum. Mutat. 34 (2013) 97.
[27] H. Lee, J.M. Graham Jr., D.L. Rimoin, R.S. Lachman, P. Krejci, S.W. Tompson, S.F. Nelson, D. Krakow, D.H. Cohn, Am. J. Hum. Genet. 90 (2012) 746.
[28] C. Michot, C. Le Goff, A. Goldenberg, A. Abhyankar, C. Klein, E. Kinning, A.M. Guerrot, P. Flahaut, A. Duncombe, G. Baujat, S. Lyonnet, C. Thalassinos, P. Nitschke, J.L. Casanova, M. Le Merrer, A. Munnich, V. Cormier-Daire, Am. J. Hum. Genet. 90 (2012) 740.
[29] S.J. Yarwood, M.R. Steele, G. Scotland, M.D. Houslay, G.B. Bolger, J. Biol. Chem. 274 (1999) 14909.
[30] G.B. Bolger, G.S. Baillie, X. Li, M.J. Lynch, P. Herzyk, A. Mohamed, L.H. Mitchell, A. McCahill, C. Hundsrucker, E. Klussmann, D.R. Adams, M.D. Houslay, Biochem. J. 398 (2006) 23.
[31] E. Stefan, B. Wiesner, G.S. Baillie, R. Mollajew, V. Henn, D. Lorenz, J. Furkert, K. Santamaria, P. Nedvetsky, C. Hundsrucker, M. Beyermann, E. Krause, P. Pohl, I. Gall, A.N. MacIntyre, S. Bachmann, M.D. Houslay, W. Rosenthal, E. Klussmann, J. Am. Soc. Nephrol. 18 (2007) 199.
[32] S.J. MacKenzie, G.S. Baillie, I. McPhee, G.B. Bolger, M.D. Houslay, J. Biol. Chem. 275 (2000) 16609.
[33] A. Robichaud, P.B. Stamatiou, S.L. Jin, N. Lachance, D. MacDonald, F. Laliberte, S. Liu, Z. Huang, M. Conti, C.C. Chan, J. Clin. Invest. 110 (2002) 1045.
[34] A.S. Kalgutkar, E. Choo, T.J. Taylor, A. Marfat, Xenobiotica 34 (2004) 755.